1 # Ammonia emission estimates using CrIS satellite observations over

2 # Europe

3 Jieying Ding[1*], Ronald van der A[1], Henk Eskes[1], Enrico Dammers[2], Mark Shephard[3], Roy

4 Wichink Kruit[4], Marc Guevara[5], Leonor Tarrason[6]

5 1. Royal Netherlands Meteorological Institute (KNMI), De Bilt, The Netherlands

6 2. Netherlands Organisation for Applied Scientific Research (TNO), Utrecht, The Netherlands

7 3. Environment and Climate Change Canada (ECCC), Toronto, Ontario, Canada

8 4. National Institute for Public Health and the Environment, Bilthoven, The Netherlands

9 5. Barcelona Supercomputing Center, Barcelona, Spain

10 6. NILU – Norwegian Institute for Air Research, Kjeller, Norway

12 *Corresponding authors: Jieying Ding (jieying.ding@knmi.nl)

15 ## Abstract

17 Over the past century ammonia (NH_3) emissions have increased with the growth of livestock and

18 fertilizer usage. The abundant NH_3 emissions lead to secondary fine particulate matter ($PM_{2.5}$) pollution,

19 climate change, reduction in biodiversity and affect human health. Up-to-date and spatially and

20 temporally resolved information of NH_3 emissions is essential to better quantify its impact. In this study

21 we applied the existing DECSO (Daily Emissions Constrained by Satellite Observations) algorithm to

22 NH_3 observations from the Cross-track Infrared Sounder (CrIS) to estimate NH_3 emissions. Because

23 NH_3 in the atmosphere is influenced by Nitrogen Oxides (NO_x), we implemented DECSO to estimate

24 NO_x and NH_3 emissions simultaneously. The emissions are derived over Europe for 2020 on a spatial

25 resolution of $0.2° \times 0.2°$ using daily observations from both CrIS and TROPOMI (on the Sentinel 5p

26 satellite). Due to the limited number of daily satellite observations of NH_3, monthly emissions of NH_3

27 are reported. The total NH_3 emissions derived from observations are about 8 Tg/year with a precision

28 of about 5-17 % per grid cell per year over the European domain [-10° ~30° E, 35° ~ 55° N]. The

29 comparison of the satellite-derived NH_3 emissions from DECSO with independent bottom-up

30 inventories and in-situ observations indicates a consistency in terms of magnitude on the country totals,

31 the results also being comparable regarding the temporal and spatial distributions. The validation of
32 DECSO over Europe implies that we can use DECSO to quickly derive fairly good monthly emissions
33 of NH_3 over regions with limited local information of NH_3 emissions.

34

35

36 1 Introduction

37

38 Ammonia (NH_3) is the most abundant alkaline gas and one of the main reactive nitrogen species in the
39 atmosphere. NH_3 is a precursor for the formation of atmospheric aerosols, which play an important role
40 in climate change. In Europe, about 50% (Wyer et al., 2022) of atmospheric NH_3 is transformed into
41 fine particulate matter ($PM_{2.5}$) composed of ammonium through chemical reactions with sulfuric and
42 nitric acids from nitrogen oxides (NO_x) and sulphur dioxides (SO_2) in the atmosphere (Renard et al.,
43 2004; Schaap et al., 2004). According to the European Environment Agency (EEA), the dominant
44 source of NH_3 in Europe is agriculture, which was responsible for more than 90% of the European
45 emissions. The other source sectors include industry, transport, energy, waste treatment and biomass
46 burning (Behera et al., 2013; Backes et al., 2016a; Van Damme et al., 2018; Adams et al., 2019).
47 Excessive NH_3 emissions have adverse impact on biodiversity, human health, and climate change
48 (Galloway et al., 2008). Over the past century, NH_3 emissions increased strongly with the growing
49 human population, cattle farming and fertilizer usage (Crippa et al., 2023; Erisman et al., 2008; Van
50 Damme et al., 2021), leading to high nitrogen deposition loads to water and soil (Erisman et al., 2013)
51 with the associated eutrophication, acidification and biodiversity loss problems (Behera et al., 2013).
52 Since 2019, the Dutch policy makers paid a lot of attention to NH_3 emissions due to the nitrogen (N)
53 crisis after the national programmatic approach to nitrogen was rejected by the supreme court, because
54 it was inadequate for the protection of vulnerable nature areas (named Natura 2000). The Dutch
55 government is obliged by EU laws to protect the natural environment and prevent damage caused by
56 too high emissions of reactive nitrogen. Studies show that abatement of NH_3 emissions is very cost-
57 effective to improve air quality and have high social benefits (Backes et al., 2016b; Zhang et al., 2020;
58 Gu et al., 2021). Detailed spatially and temporally resolved information of NH_3 emissions is crucial for
59 both scientific communities and policy makers to study and predict pollutant concentrations and
60 deposition with their impact on the environment and to motivate environmental control strategies.

61 The empirical method to estimate NH_3 emissions is the so-called bottom-up approach, which combines
62 available official reported activity data incorporating a full differentiation of emission activities with
63 emission factors, and technology and abatement measures from individual countries for each source
64 category (Crippa et al., 2018; Crippa et al., 2023; Janssens-Maenhout et al., 2019). The annual emissions

65 are then distributed in time and space based on proxy data such as land use data, and meteorological

66 parameters (Backes et al., 2016a). Ge et al. (2020) summarized the key factors of agricultural NH_3

67 emissions: local agricultural practices, manure and fertilizer application including type, amount and

68 method, animal species, housing, manure storage, meteorological conditions, soil properties, and

69 regulations of agricultural practice. The uncertainties of NH_3 emissions calculated by the bottom-up

70 approach are very large due to insufficient data on agricultural activities (Behera et al., 2013; Beusen

71 et al., 2008). Crippa et al. (2018) pointed out that the uncertainty of NH_3 (between 186 % and 294.4 %)

72 in the EDGAR (The Emissions Database for Global Atmospheric Research) inventory is the largest

73 among all pollutants because of the high uncertainty of both agricultural statistics and emission factors.

74 The validation of NH_3 emission inventories using ground-based observations is very challenging due

75 to the sparsely distributed in-site measurement network. NH_3 concentrations have large temporal and

76 spatial variability due to its short lifetime, which ranges from about a few hours to two days (Dammers

77 et al., 2019; Luo et al., 2022). Densely distributed hourly or daily ground measurements are impractical

78 for large areas due to high costs and specific operational requirements (Noordijk et al., 2020). In the

79 last decade, a wide spatial and temporal coverage of satellite observations of NH_3 in lower troposphere

80 was established due to the development of infrared nadir viewing satellite instruments, such as the

81 Tropospheric Emission Spectrometer (TES) (Beer et al., 2008) on the NASA Aura satellite. The

82 operational Cross-track Infrared Sounder (CrIS) (Shephard and Cady-Pereira, 2015) on the Suomi

83 National Polar-orbiting Partnership (S-NPP) and on the Joint Polar Satellite System-1 and System-2

84 (JPSS-1 and JPSS-2, also named as NOAA-20 and NOAA-21) satellites of NASA/NOAA, and the

85 Infrared Atmospheric Sounder Interferometer (IASI) (Clarisse et al., 2009) on the MetOp satellites from

86 the European Space Agency (ESA), with their large swaths, provide daily global coverage of NH_3

87 observations and improve our understanding of NH_3 global distribution and temporal variability.

88 NH_3 emissions can be obtained by applying an inversion algorithm to satellite observations. Such

89 estimates provide useful information which is independent from bottom-up inventories. By using IASI

90 NH_3 observations, Van Damme et al. (2018) identified NH_3 emission hotspots and calculated emissions

91 based on a mass balance approach. They found that NH_3 emissions of most hotspots, especially

92 industrial emitters, were largely underestimated compared to EDGAR. Dammers et al. (2019) used both

93 IASI and CrIS observations to derive emissions, lifetimes and plume widths of NH_3 from large

94 agricultural and industrial point sources and concluded that 55 locations were missing in the

95 Hemispheric Transport Atmospheric Pollution version 2 (HTAPv2) emission inventory. Besides the

96 studies on point sources, data assimilation techniques combining a chemical transport model (CTM)

97 with satellite observations are also widely used to derive NH_3 surface emissions. van der Graaf et al.

98 (2022) adjusted the NH_3 emissions over Europe using a local ensemble transport Kalman filter (LETKF)

99 applied to CrIS NH_3 profiles. Sitwell et al. (2022) developed an ensemble-variational inversion system

100 to estimate NH_3 emissions from CrIS over North America. Another widely used method is 4D-Var

using the GEOS-Chem global chemistry transport model, which has been applied to America, China and Europe using NH_3 observation from different instruments (Zhu et al., 2013; Zhang et al., 2018; Li et al., 2019; Cao et al., 2020; Chen et al., 2021; Cao et al., 2022). The main advantage of CrIS is the combination of global coverage and the improved sensitivity in the boundary layer attributed to the low spectral noise of about 0.04 K at 280 K in the NH_3 spectral band (Zavyalov et al., 2013). The infrared instrument is also more sensitive at the overpass time in the early afternoon with high thermal contrast between air and surface.

The Daily Emissions Constrained by Satellite Observations (DECSO) inversion algorithm uses satellite column observations to derive emissions for short-lived gases based on an extended Kalman Filter (Mijling and van der A, 2012). The concentrations of the species are calculated from the emissions by a CTM and compared to satellite observations. One of the main advantages to use DECSO is the fast calculation speed compared to other data assimilation methods. Furthermore, the derived emissions are updated by addition, not by scaling the existing emissions. This enables the fast detection of new sources and changed emissions. In previous studies, DECSO has been applied to nitrogen dioxide (NO_2) observations from different satellites and uses the Eulerian regional off-line CTM CHIMERE (Menut et al., 2021; Menut et al., 2013) to estimate regional NOx (NO_2+NO) emissions and it revealed that the temporal and spatial variability of total surface NO_x emissions are well captured by DECSO compared to bottom-up inventories or in-situ observations (Ding et al., 2015; Ding et al., 2017b; Ding et al., 2020; van der A et al., 2020; Ding et al., 2022; Liu et al., 2018).

Direct validation of emission inventories, regardless of bottom-up or satellite-derived approaches, presents the same challenge due to the inherent difficulty of directly measuring large-scale emissions on the ground. The intercomparison of emissions using independent data and different approaches are usually performed to assess the emission data. Another common way to validate emissions can be achieved by using them as input data in a chemical transport model. The model simulated concentrations are compared to in-situ observations.

In this study we extend the DECSO-NOx system to NH_3 in order to derive both NO_x and NH_3 emissions simultaneously, using CrIS NH_3 observations and NO_2 observations from the TROPOspheric Monitoring Instrument (TROPOMI) (Veefkind et al., 2012). Using the multi-species DECSO version, we update NO_x and NH_3 emissions simultaneously to reduce the impact of the temporal change (e.g. trend) of NO_x when deriving NH_3 emissions. After the description of the DECSO algorithm applied to NH_3, the results of NH_3 emissions over Europe are presented at a spatial resolution of $0.2° \times 0.2°$. To evaluate the derived NH_3 emissions, we will compare the country totals and the monthly variability with bottom-up inventories with a focus on NH_3 emissions in the Netherlands. In addition, we compare the NH_3 concentration simulations of CHIMERE using different emission inventories with in-situ observations.

136

2 Data and Method

2.1 Satellite observations

2.1.1 CrIS observations of NH$_3$

The CrIS instrument is a Fourier transform spectrometer (FTS) launched on the Suomi National Polar-orbiting Partnership (SNPP) satellite in 2011 and on the NOAA-20 satellite in 2017. The overpass time of SNPP at the equator is about 01:30 and 13:30 local time. NOAA-20 circles the earth in the same orbit as SNPP, but it is separated in time and space by 50 minutes and crosses the equator at about 02:20 and 14:20 local time. The instrument has a wide swath of up to 2200 km providing twice daily global coverage. The total angular field-of-view consists of a 3×3 array of circular pixels of 14 km diameter each at nadir (Han et al., 2013). CrIS measures the infrared spectrum including the main NH$_3$ spectral signatures located in the longwave window region between 900 and 1000 cm^{-1}. The spectral resolution of the radiance data is 0.625 cm^{-1}. NH$_3$ observations are retrieved with the CrIS Fast Physical Retrieval (CFPR) algorithm based on an optimal estimate method minimizing the difference between measured spectral radiances and those simulated by a radiative transfer model (Shephard and Cady-Pereira, 2015). Three typical a priori profiles of NH$_3$ representing high-source, moderate-source and background source are used in the retrieval algorithm. The NH$_3$ profiles are retrieved on 14 pressure levels with the peak sensitivity of CrIS between 900 and 700 hPa (Shephard et al., 2020). For SNPP, the retrieval products start from 2011 and ends in May 2021 with missing data from April to August in 2019. The NH$_3$ retrieval product of NOAA-20 starts from March 2019. We use the version 1.6.4 retrieval products of CrIS on both SNPP and NOAA-20 from September 2019 to December 2020, which also accounts for non-detects in the observations and retrievals through optically thin clouds (White et al., 2023). We use the daytime observations with the quality flag larger than 3 over our study domain of Europe [-10° ~30° E, 35° ~ 55° N] (Shephard et al., 2020). Since there are almost no emissions over ocean, we only use the observations over land. To reduce extreme emission updates in one day we filter the NH$_3$ data larger than the value at 99th percentile of all observations for the selected period over the study domain. This has also been applied by van der Graaf et al. (2022). To make a fair comparison between NH$_3$ observations of CrIS and model simulations of CHIMERE, we interpolate modelled concentrations from the model grid cell over the satellite footprints and apply the averaging kernel to the modelled profile. Although the NH$_3$ observations from CrIS are in circular pixels, we still assume the pixel to be rectangular and calculate the pixel corner coordinates based on the satellite height, satellite zenith angle and viewing angle assuming the width of the pixel to be equal to the diameter of the circular pixel. To simplify the calculation of applying the original logarithmic averaging kernels, we converted them to linearized average kernels based on the method of Cao et al. (2022).

170

2.1.2 TROPOMI observations of NO₂

TROPOMI is onboard the Sentinel-5 Precursor (S5P) satellite launched on 13 October 2017 with the high spatial resolution of 3.5×5.5 km^2 at nadir for the NO_2 observations. The overpass time is about 13:30 local time, similar as for CrIS. We use TROPOMI tropospheric NO_2 columns from the version 2.4 reprocessed retrieval dataset (van Geffen et al., 2022) and follow the recommendations for using the QA value as detailed in the Product User Manual (Eskes and Eichmann, 2022). NO_2 columns are converted into 'super-observations' representing the integrated average (Boersma et al., 2016; Rijsdijk et al., 2024) over the $0.2° \times 0.2°$ grid cells. The super-observation error takes into account spatial correlations between individual TROPOMI observations and representativity errors in the case of incomplete coverage. In this paper, the super-observations are calculated for the NO_2 columns from surface till about 700hPa where the NO_2 concentrations are most related to surface emissions. The signal-to-noise ratio and calculation time of DECSO are improved by using super-observations. The details of TROPOMI NO_2 data used by DECSO are described in Ding et al. (2020) and van der A et al. (2024).

185

2.2 Ground-based observations.

To evaluate the NH_3 emissions derived by DECSO, we use independent ground-based observations in 2020 to compare with model simulated NH_3 concentrations of CHIMERE using different inventories. Compared to other countries, Netherlands has the densest network for monitoring surface NH_3 concentrations. We use hourly NH_3 concentrations measured by mini-DOAS at six locations (Figure S1) from the Dutch Monitoring Air Quality (LML) network (Berkhout et al., 2017) and monthly measurements of NH_3 concentration provided by passive samples at 394 locations (Figure S2) from the Dutch Measuring Ammonia in Nature (MAN) network (Lolkema et al., 2015). The uncertainty in NH_3 concentrations measured with individual passive samples is large (22% for a single monthly measurement) and the measurements are calibrated monthly against the high-quality measurements (about 20% for an hourly measurement) from the LML network to enhance the accuracy.

197

2.3 Emission inventories

To verify the satellite-derived emissions of NH_3 in Europe, we compare them to several emission inventories including: the national emissions inventories officially reported under the Convention on Long-range Transboundary Air Pollution (LRTAP) (Pinterits, 2023) of 2020, the emissions reported under the European Pollutant Release and Transfer Register (E-PRTR) (EPRTR, 2012) of 2020

including releases from industrial facilities and livestock facilities, the global emission inventory Hemispheric Transport of Air Pollution (HTAP) v3 of 2018 (Crippa et al., 2023), the Copernicus Atmosphere Monitoring Service (CAMS) Global anthropogenic emissions (CAMS-GLOB-ANT) v5.3 of 2020 (Soulie et al., 2023), the regional European CAMS anthropogenic emission inventory (CAMS-REG-ANT) v5.1 of 2020 (Kuenen et al., 2022) and the Dutch official registered emissions of NH_3 in 2020 (https://data.emissieregistratie.nl/export) (see Table 1). HTAP v3 has been developed by integrating official inventories over specific areas including CAMS-REG-ANT v5.1 for Europe with the EDGAR v6.1 inventory for the remaining world regions with the spatial resolution of $0.1° \times 0.1°$. CAMS-GLOB-ANT combines the EDGAR annual emissions and the Copernicus Atmosphere Monitoring Service TEMPOral profiles (CAMS-TEMPO) on a global scale (Guevara et al., 2021). The emissions of the most recent years are calculated based on the trends from the Community Emissions Data System (CEDS) global inventory (Hoesly et al., 2018). The resolution of CAMS-GLOB-ANT is $0.1° \times 0.1°$. CAMS-REG-ANT v5.1 provide yearly emissions on the spatial resolution of $0.1° \times 0.05°$. We have applied the regional European CAMS-TEMPO profiles (Guevara et al., 2021) to CAMS-REG-ANT v5.1 to get the monthly emissions (hereinafter referred to as CAMS-REG-TEMPO). The Dutch registered NH_3 emissions are taken from https://www.emissieregistratie.nl and provided annually on a high resolution of 1 km ×1 km. To compare the derived NH_3 emissions of DECSO spatially with bottom-up inventories, we aggregate emissions from these bottom-up inventories into the $0.2° \times 0.2°$ grid cells of the DECSO working domain.

Table 1. Summary of the bottom-up inventories compared to the satellite-derived NH_3 emissions from DECSO.

Emission inventory	Year	Spatial Resolution	Temporal resolution
LRTAP	2020	Country total	Annual
E-PRTR	2020	Point source	Annual
HTAP v3	2018	$0.1° \times 0.1°$	Monthly
CAMS-GLOB-ANT v5.3	2020	$0.1° \times 0.1°$	Monthly
CAMS-REG-ANT v5.1	2020	$0.1° \times 0.05°$	Annual, monthly (with CAMS-REG-TEMPO)
Dutch Registered NH_3 emissions	2020	1 km ×1 km	Annual

2.4 DECSO

DECSO is an inversion algorithm developed for the purpose of deriving emissions of short-lived species from satellite observations. As such DECSO has been specifically designed to use daily satellite observations of column concentrations to provide rapid updates of emission estimates of short-lived atmospheric constituents on a regional scale. An extended Kalman filter is used, in which emissions are translated to column concentrations via the CTM and these are compared to the satellite column observations. Based on that single forward CTM simulation, the sensitivity of concentrations to emissions is calculated by using trajectory analyses to account for transport away from the source. In previous studies, DECSO has been applied to NO_2 observations from different satellites including TROPOMI to estimate NO_x emissions (Mijling et al., 2013; Ding et al., 2015; van der A et al., 2020; Ding et al., 2022; Ding et al., 2020; van der A et al., 2024). The studies revealed that the temporal and spatial variability of total surface NO_x emissions are captured well by DECSO (Ding et al., 2017b; van der A et al., 2017; Liu et al., 2018; van der A et al., 2024). Here we have used the updated version DECSO v6.3 (van der A et al., 2024) for estimating simultaneously NO_x and NH_3 emissions using the daily observations from TROPOMI and CrIS (referred to as multi-species DECSO). The main changes of v6.3 include improving the sensitivity matrix calculation and using the latest Eulerian regional off-line CTM CHIMERE v2020v3 (Menut et al., 2021) instead of CHIMERE v2013. In the CTM, we employ the Copernicus Landcover 2019 data (Buchhorn et al., 2020) , and the source sector distributions of emissions obtained from HTAP v3 of 2018, which are also used as input emissions of other species beside NO_x and NH_3. CHIMERE is driven by the operational meteorological forecast of the European Centre for Medium-Range Weather Forecasts (ECMWF). Here we present the specific setting in DECSO for NH_3 (referred to as DECSO-NH3).

To update NH_3 emissions based on the Kalman filter equations, one of the essential calculations is the Kalman gain matrix (**K**) using the following equation:

$$\mathbf{K} = \mathbf{P}^f(t)\mathbf{H}[\mathbf{H}\mathbf{P}^f(t)\mathbf{H}^T + \mathbf{R}]^{-1} \qquad (1)$$

$\mathbf{P}^f$ is the error covariance matrix of the forecasted emissions at time t. **H** is the sensitivity matrix (Jacobian) describing how the NH_3 column concentration on a satellite footprint depends on gridded NH_3 emissions. **R** is the error covariance combining the observation error of tropospheric NH_3 columns, the uncertainty of the CTM, and representation error introduced by projection of modelled columns on the satellite footprint.

$\mathbf{P}^f$ is parametrised based on an evaluation of the emission forecast error q, which is the error increase during one time step of the forecast model. The emission forecast model is persistence, predicting that the emission is equal to the analysis of the emissions from the previous day. We parametrize q of NH_3 following:

259 $$q = \varepsilon_{abs} \exp\left(-\frac{\varepsilon_{rel}}{\varepsilon_{abs}} e\right) + \varepsilon_{rel} e \qquad\qquad (2)$$

260 ε_{abs} and ε_{rel} are the absolute and relative errors that are the dominating emission errors for low and high

261 emissions respectively.

262 To determine ε_{abs}, ε_{rel} and also the covariance matrix **R** for NH$_3$, we follow the method described by

263 Ding et al. (2017a) based on the analysis of Observation minus Forecast (OmF) and Observation minus

264 Assimilation (OmA). The fitted ε_{abs}, ε_{rel} are 0.075×10^{15} molecule cm^{-2} h^{-1} and 0.045. Note that **R** is the

265 variance of the observation error, the CTM model error and the representation error. Our analyses

266 showed that the **R** values are dominated by the satellite observation errors (σ_{obs}). The representation

267 error can be neglected. We set the small contribution of model errors in **R** to 0.5×10^{15} molecule cm^{-2}.

268 To capture the quick changes of NH$_3$ emissions during the fertilizing seasons and give more weight to

269 satellite observations with high values during the assimilation, we need to reduce their high observation

270 errors for high values and keep the same observation errors for low values. By fitting NH$_3$ observation

271 errors (σ_{obs}) against the observed columns C using all observations in 2020, we find a linear relation:

272 $$\bar{\sigma}_{obs} = \alpha C + b \qquad\qquad (3)$$

273 α is equal to 0.2 and b is equal to 1×10^{15} molecule cm^{-2}. If the given σ_{obs} is larger than $\alpha C + b$, we

274 use Eq (3) for the observation error in **R**.

275 We update NH$_3$ emissions only over land since there are almost no NH$_3$ emissions over oceans and seas.

276 As we mentioned, NH$_3$ reacts with sulfuric and nitric acids from SO$_2$ and NO$_x$ to form PM$_{2.5}$. The

277 changes in NO$_x$ and SO$_2$ emissions will affect the concentration and removal of NH$_3$ in the atmosphere.

278 Inaccurate emissions of NO$_x$ and SO$_2$ will therefore affect the inversion of NH$_3$ emissions (Kuttippurath

279 et al., 2024). To assess the sensitivity of NH$_3$ emissions derived with DECSO on NO$_x$ and SO$_2$ emissions,

280 we have run DECSO with different NO$_x$ and SO$_2$ emissions (default emissions of HTAP v3 and

281 doubling the emissions of HTAP v3 for SO$_2$ and NO$_x$) as input for the CTM. The results shows that the

282 inversion of NH$_3$ emissions is not sensitive to the change of SO$_2$ emissions, but it is to NO$_x$ emissions.

283 In Europe, the impact of SO$_2$ emissions on NH$_3$ can be neglected nowadays due to the low SO$_2$

284 emissions (Luo et al., 2022), which have been reduced by 80% in 2020 compared to 2005 (EEA, 2023).

285 The sensitivity tests indicate that up-to-date NO$_x$ emissions are very important for the accurate inversion

286 of NH$_3$ emissions. The monthly NO$_x$ emissions of HTAP in 2018 and derived with DECSO in 2020 are

287 quite different over the various countries (Figure S3). In 2020, due to the COVID-19 pandemic, NO$_x$

288 emissions reduced compared to other years. van der A et al. (2024) has compared the seasonality of

289 NO$_x$ emissions of DECSO to other bottom-up inventories and showed individual temporal variability

290 of industrial facilities is derived with DECSO in Europe, while bottom-up inventories use the same

291 temporal profile per country per sector and no detailed information of the temporal changes of

292 individual sources. We estimate NH$_3$ and NO$_x$ emissions with DECSO simultaneously (the multi-specie

293 DECSO) from CrIS and TROPOMI on a daily basis. We use the DECSO-NH3 version to estimate only

294 NH$_3$ emissions from CrIS and use NO$_x$ emissions of HTAP v3 as input for the CTM. Figure 1 shows

295 the difference of monthly NH$_3$ emissions in three countries (Netherlands, Italy and Greece) derived with

296 the multi-species DECSO version and the DECSO-NH3 version. The derived NH$_3$ emissions all differ

297 largely (up to ±40%) in winter and less in summer.

298
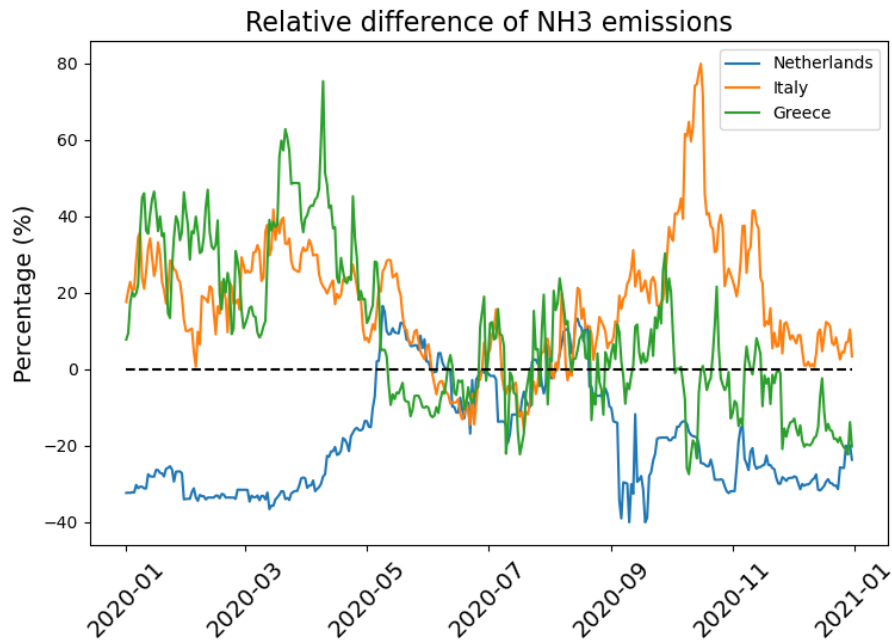
299

300 *Figure 1. The relative difference (multi-species DECSO minus DECSO-NH3) of NH$_3$ emissions between multi-species DECSO and*

301 *DECSO-NH3. DECSO-NH3 means that only NH$_3$ emissions are derived with CrIS-NOAA-20. multi-species DECSO means that*

302 *NH$_3$ and NO$_x$ emissions are derived using CrIS-NOAA-20 and TROPOMI observations.*

303 3. Results

304 3.1 NH$_3$ emissions in Europe

305 We have run the multi-species DECSO version with NH$_3$ observations from CrIS-NOAA-20 and CrIS-

306 SNPP respectively to estimate NH$_3$ emissions over the selected domain of Europe in 2020 (Figure 2),

307 which is the only year with a full year overlap of NH$_3$ observations for these two satellites. The total

308 NH$_3$ emissions over the study domain are 8.0 Tg/year from SNPP and 8.1 Tg /year from NOAA-20.

309 The spatial distribution of the NH$_3$ emissions derived from the two satellites agrees well, with small

310 differences (with a relative root mean square difference of 1.2%) resulting from deviations of the

311 observed NH$_3$ columns. The spatial distribution of high NH$_3$ emissions derived from DECSO is similar

312 to that of HTAP, CAMS-REG-ANT and CAMS-GLOB-ANT but with more local-scale variability and

hotspots. The total emissions of DECSO over the European domain are higher than HTAP (4.2 Tg/year), CAMS-REG-ANT (4.0 Tg/year) and CAMS-GLOB-ANT (5.9 Tg/year)
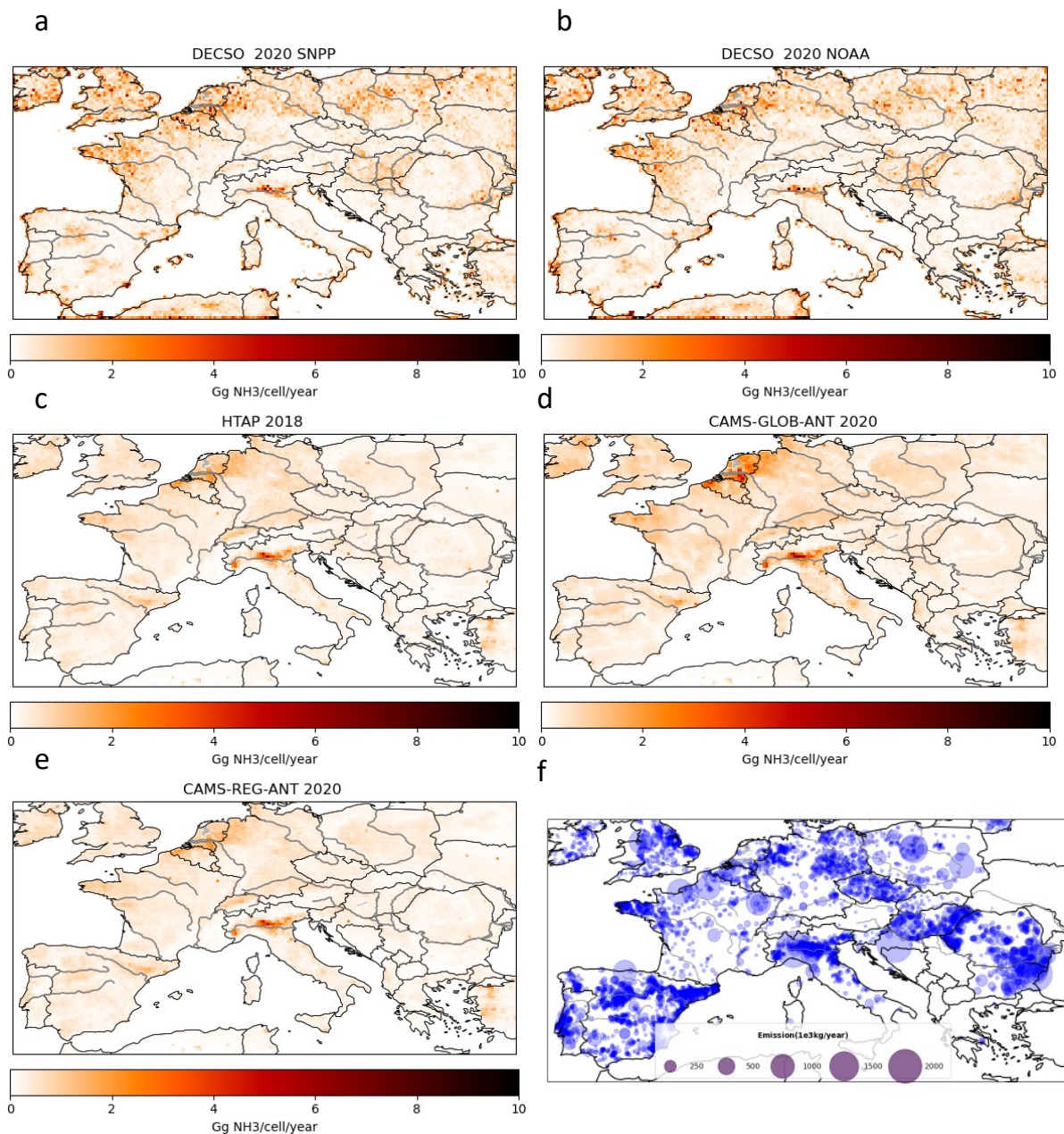
Figure 2. NH$_3$ emission maps. NH$_3$ emissions derived with DECSO from (a) SNPP and (b) NOAA-20 in 2020. NH$_3$ emissions of (c) HTAP in 2018, (d) CAMS-GLOB-ANT in 2020 (e) CAMS-REG-ANT in 2020. (f) The registered point sources of E-PRTR in 2017.

The locations of high NH$_3$ emissions, especially in Po-Valley, Spain, Hungary and the east of Romania, shown in DECSO are highly corelated to the registered NH$_3$ point sources of E-PRTR which are from industrial facilities including livestock facilities but not from fertilizer applications. We see that emissions from the Netherlands are high in DECSO and the bottom-up inventories but are missing in the database of E-PRTR. For the countries in East Europe (e.g. Poland, Hungary, Romania), the NH$_3$

emissions derived with DECSO are much higher than from the bottom-up inventories. To assess the NH$_3$ emissions per country, we calculated the country total emissions (see Figure 3). The correlation coefficients of country totals from DECSO with the bottom-up inventories are all higher than 0.95. In general, the country totals of NH$_3$ emissions derived by DECSO from either NOAA-20 or SNPP are comparable to HTAP, LRTAP, CAMS-REG-ANT and CAMS-GLOB-ANT, with DECSO about 30% higher. HTAP, LRTAP and CAMS-REG-ANT have very similar emissions per country, while CAMS-GLOB-ANT shows higher emissions than the other three bottom-up inventories. Because HTAP v3 uses annual emissions from CAMS-REG-ANT for Europe, the only difference between HTAP v3 and CAMS-REG-ANT is the difference in year. The input of CAMS-REG-ANT is mainly based on LRTAP. CAMS-GLOB-ANT is based on EDGAR and use different emission activities and factors compared to the other three bottom-up inventories. In the North part of Europe, for example Netherlands and Germany, DECSO results show lower NH$_3$ emissions than CAMS-GLOB-ANT but higher than HTAP, LRTAP and CAMS-REG-ANT.
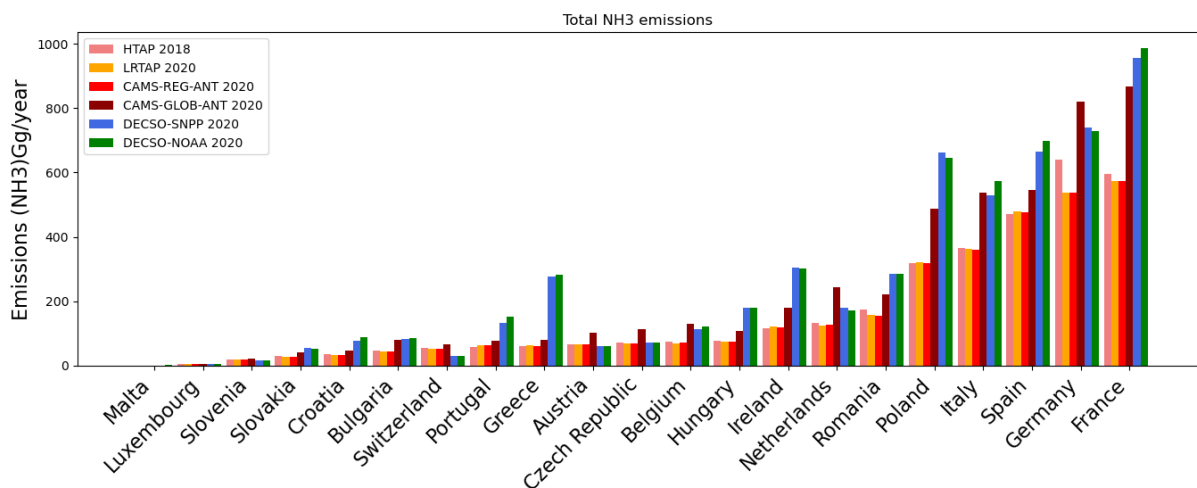
Figure 3 Country totals of NH$_3$ emissions (Gg/year) according to database LRTAP in 2020, bottom-up inventories HTAP in 2018, CAMS-REG-ANT in 2020, CAMS-GLOB-ANT in 2020 and the DECSO calculations from SNPP and NOAA-20 in 2020.

To analyze the seasonality of NH$_3$ emissions derived from DECSO, we compare the monthly emissions of DECSO with bottom-up inventories. Figure 4 shows the monthly NH$_3$ emissions from DECSO, HTAP, CAMS-REG-TEMPO, and CAMS-GLOB-ANT of the Netherlands, Spain, France and Poland. We see that the seasonal cycle of NH$_3$ emissions of DECSO is closer to CAMS-GLOB-ANT. HTAP shows the exact same monthly variability for each country. CAMS-REG-TEMPO shows very similar monthly patterns to the ones reported by CAMS-GLOB-ANT as they are both using the same method to derive the temporal profiles for livestock and agricultural soil emissions (Guevara et al., 2021). In the Netherlands as an example for north Europe, the monthly NH$_3$ emissions of DECSO are lower than

349   CAMS-GLOB-ANT but very close to CAMS-REG-ANT. Two peaks of NH_3 emissions show up in
350   April and August for CAMS emissions. This is also confirmed by the monthly surface concentrations
351   measured by the MAN network (Figure S4). In Spain and France, the monthly emissions of DECSO
352   are comparable to CAMS-GLOB-ANT. In the east part of Europe, such as Poland, DECSO estimates
353   higher emissions. Note that in spring, when the NH_3 emissions are high due to fertilizer applications on
354   farms, the NH_3 emissions derived with DECSO can suffer from a time lag due to insufficient
355   observations (e.g. due to cloudiness, see Figure S5).
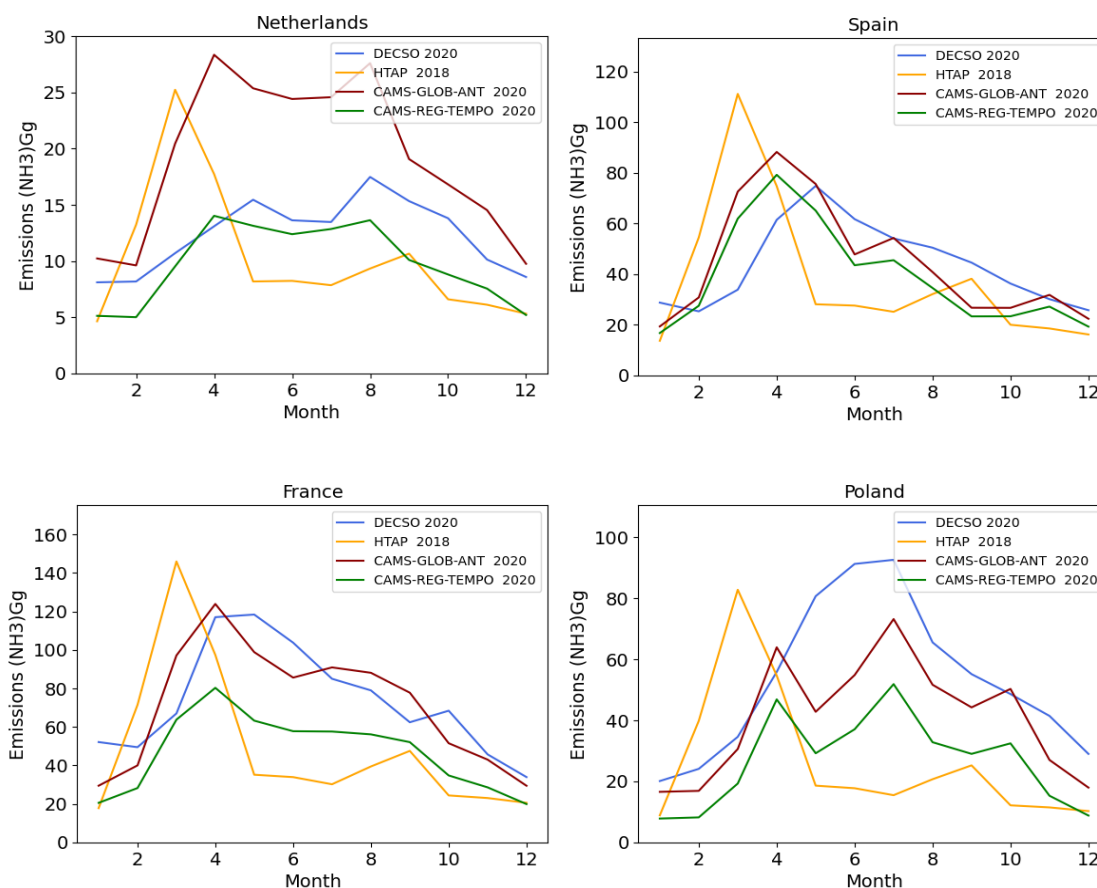
356

357   *Figure 4 Monthly NH_3 emissions (Gg/month) of DECSO in 2020, HTAP in 2018, CAMS-REG-TEMPO in 2020 and CAMS-GLOB-*
358   *TEMPO in 2020 for (a) the Netherlands, (b) Spain, (c) France and (d) Poland.*

359

360   3.2 Emissions in the Netherlands

361   On the emission maps of Figure 2, we see that the Netherlands and Po-valley have the highest emission
362   intensity of NH_3. In this section, we focus our analysis on the Netherlands since it has the densest
363   network for monitoring surface NH_3 concentrations and also a detailed emission inventory on a very
364   high spatial resolution. The total emissions of the Netherlands estimated from the two satellites are very
365   similar (Figure 3), but the spatial distributions show significant differences (Figure S6). One possible
366   reason is that about 10% more observations are available from NOAA-20 than SNPP in 2020 (see Figure

367   S7). The number of valid observations is in general low at high latitudes (Figure S8). More observations

368   allow the detection of fast changes of NH_3 emissions from day to day. By averaging the emissions, the

369   information from both satellites is combined and improved the quality of the derived emissions due to

370   a doubling of the number of observations. We use the average of the results of DECSO-SNPP and

371   DECSO-NOAA-20 to get a better spatial distribution of NH_3 emissions derived from satellite

372   observations.

373   We compare the total NH_3 emissions of DECSO with CAMS-GLOB-ANT, HTAP and official national

374   NH_3 emissions of the Netherlands, which are 148, 230, 122 and 123 Gg/year respectively. DECSO is

375   lower than CAMS-GLOB-ANT but higher than HTAP and the official NH_3 emissions of the

376   Netherlands. Figure 5 shows the spatial distribution of each inventory in the Netherlands. We see that

377   DECSO captures the high emission areas and regional distribution over the country. The correlation

378   coefficients of the spatial distribution of NH_3 emissions between DECSO and the national emissions of

379   the Netherlands, HTAP v3, CAMS-GLOB-ANT are 0.87, 0.87 and 0.88 respectively. At the resolution

380   of the individual DECSO grid cells, $0.2° \times 0.2°$ grid cell, the emission patterns show differences. This

381   may be due to uncertainties in the location of the emissions and displacements by up to one grid cell,

382   similar as for NO_x emissions (van der A et al., 2024). For example. the emission sources at the edge of

383   grid cells can be spread to the neighbouring grid cells.

384
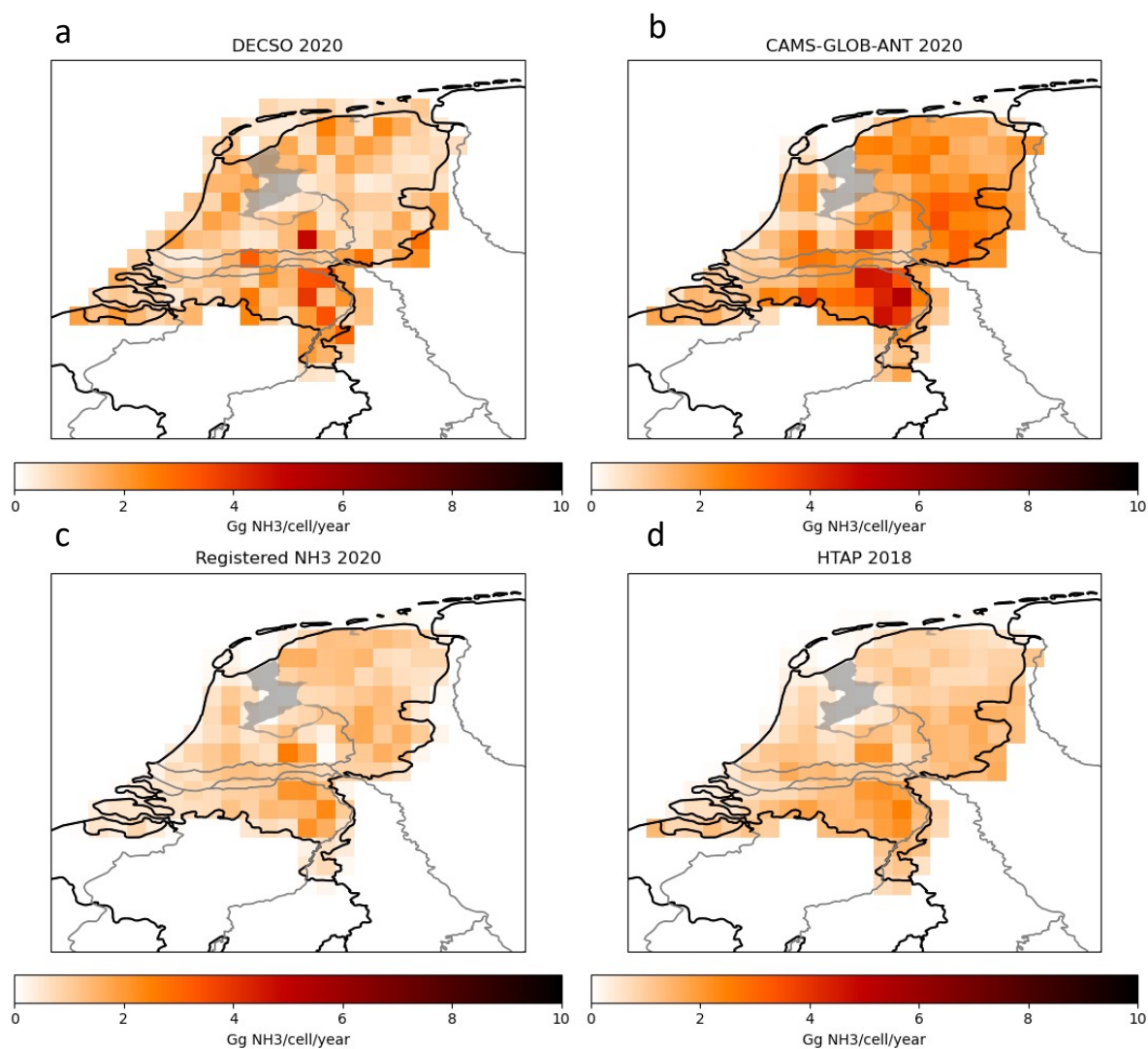
Figure 5 NH₃ emissions in the Netherlands. (a) The averaged NH₃ emissions derived with DECSO from SNPP and NOAA-20.

(b) NH₃ emissions of CAMS-GLOB-ANT in 2020. (c) The official national NH₃ emissions for the Netherlands in 2020 (from

emissieregistratie.nl). (d) NH₃ emissions of HTAP in 2018.

To further assess the DECSO results using in-situ observations from both LML and MAN networks in the Netherlands, we have conducted three runs of CHIMERE for the year 2020 using NH_3 emissions from DECSO in 2020, HTAP in 2018 and CAMS-GLOB-ANT in 2020 over the European domain (same as the setup of DECSO). To compare to the surface NH_3 measurement from the MAN network, we calculate the monthly average of surface NH_3 concentrations from the model simulations. Figure 6 (a-c) shows the scatter plots of monthly NH_3 concentrations of model simulations against observations for the whole year. We see that modelled NH_3 concentrations with the HTAP emissions are underestimated and those with the CAMS-GLOB-ANT emissions are overestimated compared to in-situ observations. The modelled NH_3 concentrations with DECSO emissions have the lowest absolute bias (modelled concentration minus in-situ observations of the MAN network) (Figure 7). The performance of model simulations is better in summer months (April to September) than in winter

399 months (October-March). In winter months, few cloud-free satellite observations are available for the

400 Netherlands. For DECSO, the scatter plot looks more spread out than in summer months (Figure 6d-i).

401 In summer months, the NH₃ concentrations with CAMS-GLOB-ANT are largely overestimated and

402 with HTAP are largely underestimated, while DECSO has a lower bias compared to the other two. Note

403 that in the grid cells, the number of stations can vary from 1 to 16. If we select grid cells with more than

404 3 sites, DECSO shows better spatial correlation with in-situ observations than for the other two

405 inventories and the lowest bias (Figure 7 and Table 2).

406
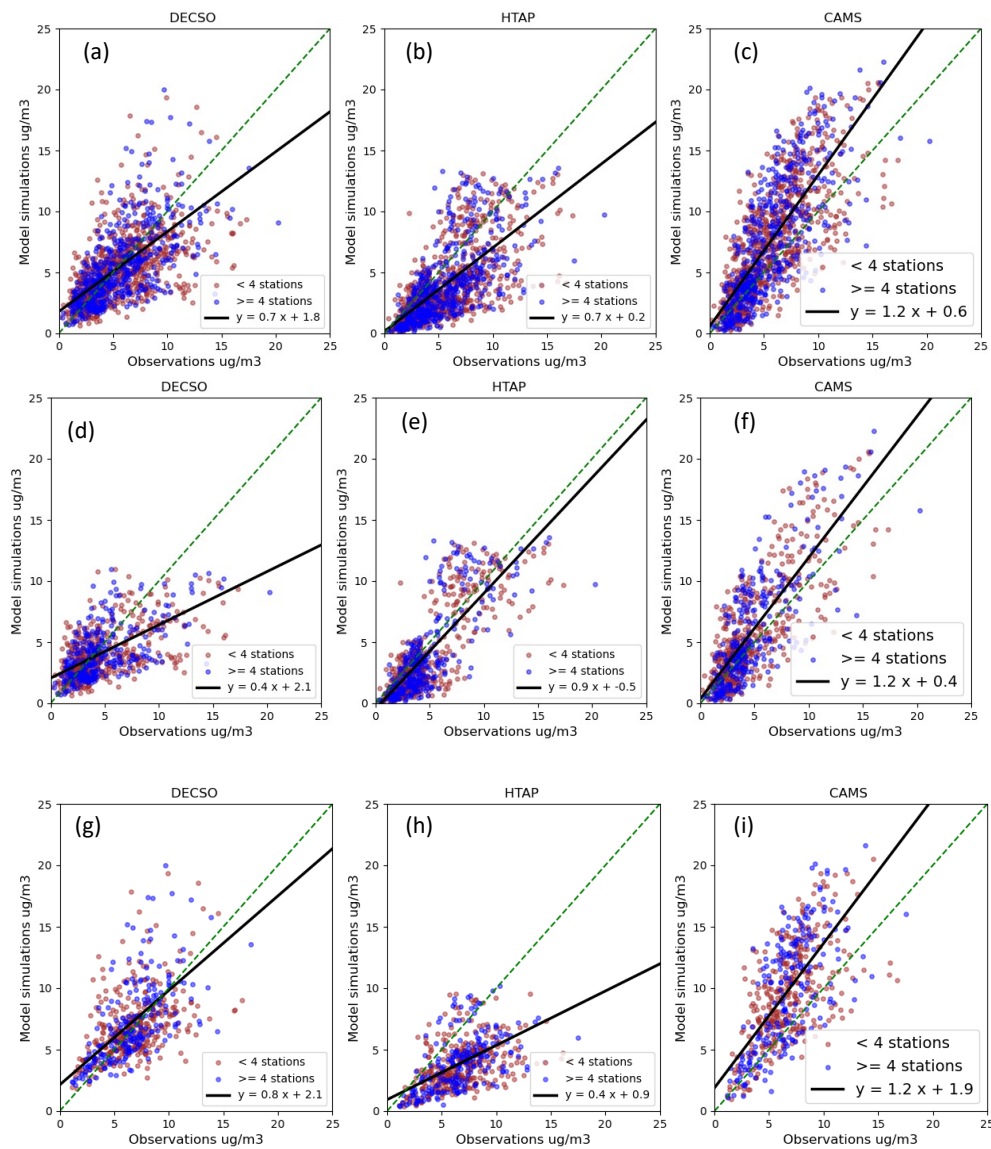
408 *Figure 6. Scatter plots of observations from the MAN network with NH₃ surface concentrations from model simulations with*

409 *NH₃ emissions from DECSO (left column), HTAP (middle column) and CAMS-GLOB-ANT (right column). (a-c) The scatter plot*

410 *of data for the whole year for all sites. (d-f) The scatter plot of the data in winter months (October to March). (g-i) The*

411 *scatter plot of the data in summer months (April to September). Each point presents the model grid cells having the in-situ*

412   *observations. The red dots mean there are less than four in-situ sites in the grid cells. The blue dots mean there are at least*
413   *four in-situ sites in the grid cell. The fitted black line is for grid cells with at least four in-situ sites.*

414
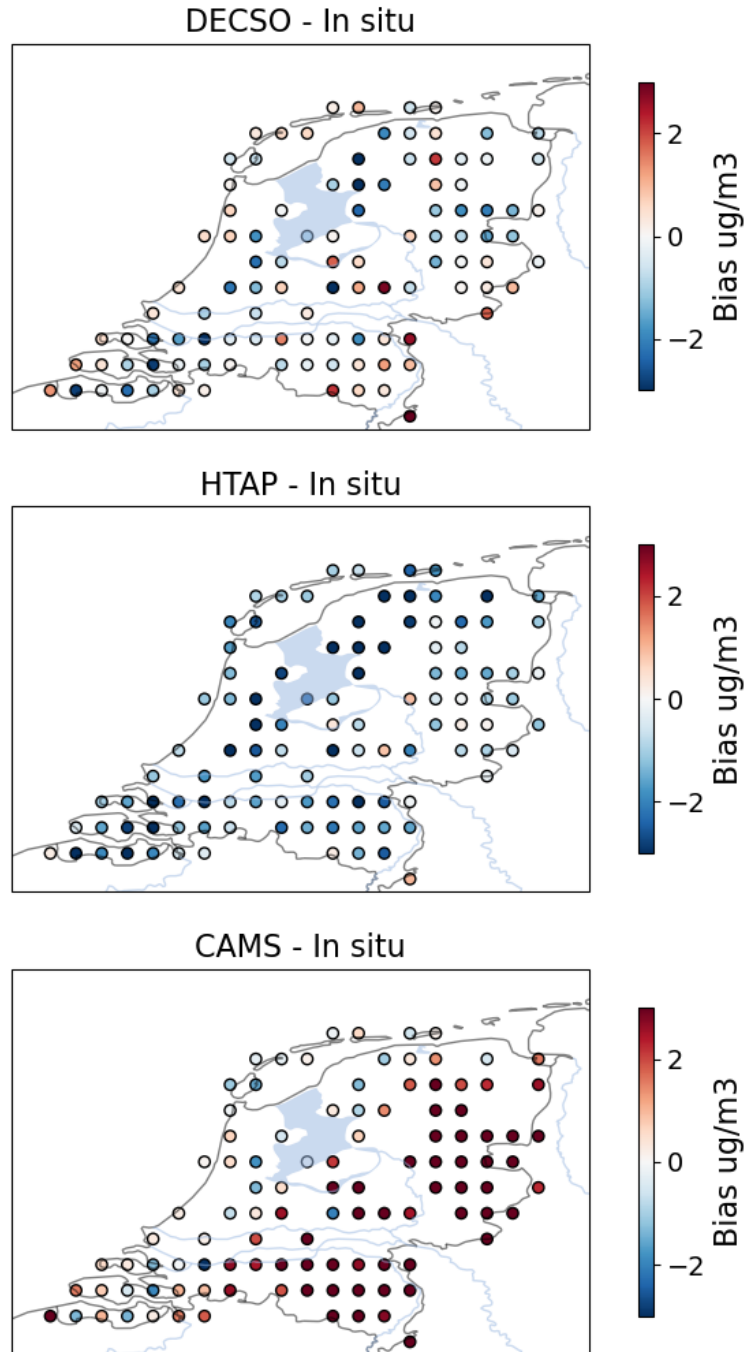
415
416   *Figure 7. Bias of the model simulated surface concentrations with NH$_3$ emissions from DECSO (left column), HTAP (middle*
417   *column) and CAMS-GLOB-ANT (right column) compared to the in-situ observations from the MAN network.*

418

Table 2. The spatial and temporal correlation coefficients and the bias of monthly mean simulated NH₃ surface concentration using DECSO, HTAP and CAMS-GLOB-ANT NH₃ emissions against observations of the MAN network for grid cells with more than three measurement locations.

	Temporal correlation coefficient	Spatial correlation coefficient	Bias (µg/m³)	RMSE (µg/m³)
DECSO	0.64	0.73	-0.2	2.6
HTAP v3	0.70	0.70	-1.9	3.0
CAMS-GLOB-ANT	0.82	0.70	-0.3	3.8

The LML network has six sites measuring surface NH_3 concentrations, which are provided every hour. Since the difference in our model simulations is only due to the monthly input emissions of NH_3, we calculate monthly average NH_3 observations for the six sites to compare with the modelled monthly averaged concentrations. The comparison shows that the model simulations using the DECSO NH_3 emissions have similar performance as bottom-up inventories (Figure S9 and S10). The correlations of modelled monthly NH_3 concentration using DECSO and CAMS-GLOB-ANT emissions with the observations from the LML network are better than that of HTAP, while CAMS-GLOB-ANT has the lowest bias. Based on these six sites, the comparison shows that the model result using DECSO is very comparable with that using CAMS-GLOB-ANT.

3.3 Uncertainties and bias of NH_3 emissions

One advantage of DECSO is that a standard deviation of derived emissions is also calculated per grid cell on a daily basis according the Kalman filter equations. As described by van der A et al. (2024), the derived errors in the emissions are correlated in time linked to the assumption of the persistent emission forecast model. The autocorrelation effects can be neglected after about one week up to ten days. We follow the autocorrelation function presented by van der A et al. (2024) to calculate the monthly variance of NH_3 emissions. The monthly variance of NH_3 emissions for each grid cell in the study domain varies from 17% to 58%. For the Netherlands, the precision (random uncertainty) of the monthly emissions is about 20% and the precision of the annual total is about 5%.

443   A bias in satellite derived emissions can be introduced due to the linearisation of the averaging kernels
444   (Sitwell et al., 2022). The CrIS ammonia observations are retrieved in logarithm space together with
445   logarithmic averaging kernels. As discussed by Sitwell et al. (2022), either using the logarithmic
446   averaging kernel or the linearized averaging kernel introduces a bias when applying them to the model
447   simulated profiles. The logarithmic averaging kernels cause problems when the model profiles are zero
448   at any point in the profile and lead to a positive bias in emission estimates. Linearized averaging kernels
449   may introduce a negative bias in emissions when there is a large difference between the model profile
450   and the a priori profile used in the retrieval.

451
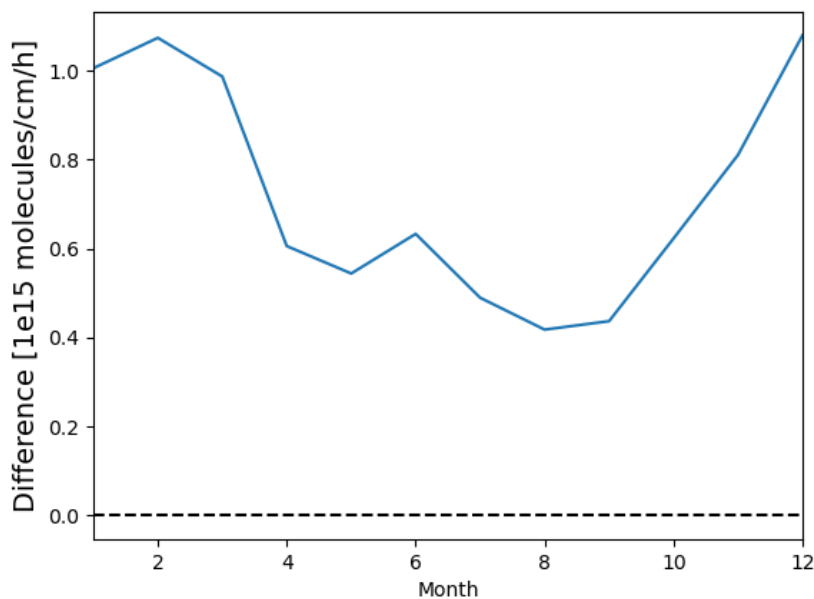
Figure 8. The absolute change of monthly NH_3 emissions (molecule/cm^2/h) if there is a positive bias of 5×10^{15} molecule/cm^2 of each NH_3 column observation.

454   To assess how the biases in satellite NH_3 observations affect emissions derived by DECSO, we have
455   done two simple bias tests. For the first test, the NH_3 columns of CrIS on NOAA-20 are increased by
456   20%, a positive relative bias for the satellite observations. The annual emissions of NH_3 with the
457   introduced bias increase by 27% for the European domain. It seems that the introduced bias has a higher
458   impact on emissions in winter than in summer. The relative bias on emissions can be as high as 50% in
459   winter. The change of emissions in summer becomes even negative probably because NH_3 column
460   concentrations can show a large variation from day to day. When the NH_3 columns are very high on
461   one day and next drop to a very low value, the absolute change in concentration is larger than the
462   original situation without introduced bias. This will lead to a larger decrease in the updated emissions
463   and can result in a negative change of emissions. For the second test, an absolute bias of 5×10^{15}
464   molecule/cm^2 is added to each NH_3 column observation of CrIS on NOAA-20. Figure 8 shows the
465   increase of NH_3 emissions caused by the absolute bias introduced in the satellite observations. We see

that the increase is doubled in winter compared to summer, because the lifetime in winter is longer than in summer. The averaged effective lifetime calculated with DECSO is about 10 hours in winter and 5 hours in summer. With the same bias of NH_3 columns, the impact on emissions is larger in winter than in summer.

4. Discussion and Conclusion

To derive NH_3 emissions from satellite data, we presented an updated version of the DECSO algorithm with specific settings for NH_3. Together with the improved the DECSO version for NO_x of van der A et al. (2024), we have the multi-species DECSO version to update NO_x and NH_3 emissions simultaneously. In general, the removal of NH_3 in the atmosphere is affected by the amount of NO_x and SO_2 emissions. For the study domain of Europe, our sensitivity study shows that the influence of changes in NO_x emissions need to be considered in the inversion of NH_3 emissions in DECSO. The impact of SO_2 emissions is very small and can be neglected since the SO_2 emissions are usually low in Europe. Thus, to derive NH_3 emissions and to analyze the seasonal cycle and trend of NH_3 emissions from satellite observations over Europe, it is recommended to include updated NO_x emissions in the inversion calculation of NH_3 emissions in DECSO. For regions with high SO_2 emissions, it is necessary to consider if the SO_2 emissions are changing rapidly and are up-to-date in the inversion.

The error covariances of the updated daily NH_3 emissions per grid cell are provided during the calculation in DECSO. Considering the autocorrelations introduced by the assumption of the persistency emission model, the calculated monthly error on NH_3 emissions for each grid cell in the study domain varies from 17% to 58%. The yearly error per grid cell is about 5 ~ 15%. The sensitivity tests for retrieval biases shows that with an introduced constant relative and absolute bias in NH_3 retrievals, the resulting bias in emissions derived with DECSO shows a seasonal variability with a peak in winter. This means the algorithm is more sensitive to a bias in the observations during wintertime.

The total NH_3 emissions in our European domain derived from NH_3 observations of SNPP and NOAA-20 are 8.0 Tg/year and 8.1 Tg/year respectively with a precision of about 5 - 17 % per grid cell/year. The difference in country total emissions derived from the two satellites is very small. However, the details of the spatial distribution of emissions derived from both satellites are different over the north part of the domain, such as the Netherlands. This may be due to the varying number of observations per region per year from the two satellites. An average of the emissions derived from both satellites leads to an improved spatial distribution compared to the emissions from the individual satellite. The spatial distribution of derived NH_3 emissions is similar to the bottom-up inventories, but DECSO emissions are in general higher. The annual total emissions derived by DECSO for the whole domain is larger than the bottom-up inventories (LRTAP, HTAP, CAMS-REG-ANT and CAMS-GLOB-ANT). The comparison of country total emissions shows that DECSO gives higher NH_3 emissions for the countries

in East Europe than the bottom-up inventories. In addition, DECSO results show higher sources in Spain, Hungary and the east of Romania. This is in line with the registered point sources of E-PRTR. The seasonal cycle of the emissions of DECSO are comparable to CAMS-GLOB-ANT, while HTAP uses the same seasonal cycle for each country in Europe. The analysis indicates that DECSO can be used to estimate NH_3 over a long period for the trend study. The retrieval product of NH_3 from SNPP ends in May 2021. Because of the insignificant differences in NH_3 emissions derived from the two satellites for the overlap year 2020, the trends analysis can be continued by using the NH_3 data from NOAA-20 (Figure S11. We have shown the importance of the impact of NO_x emissions on the inversion of NH_3 emissions. Since the NO_x emissions derived from TROPOMI have good agreement with CAMS-REG-ANT, as shown by van der A et al. (2024). the NO_x emissions from CAMS-REG-ANT can be used for the years before 2019 in trend studies of NH_3 emissions over Europe.For the Netherlands, model simulations using NH_3 emissions from DECSO, HTAP and CAMS-GLOB-ANT are compared to in-situ observations from the MAN and LML networks. In general, the simulation using DECSO emissions has a lower bias, but also a lower temporal correlation compared to CAM-GLOB-ANT. The performance of model simulations with DECSO is better in summer than in winter. Both the bias and spatial correlation between model simulations using DECSO emissions and the MAN in-situ observations are higher than CAMS-GLOB-ANT for grid cells including more than 3 measurement sites. We conclude that satellite-derived emissions derived with DECSO show a comparable temporal and spatial distribution as bottom-up inventories. The emissions derived from satellite observations can provide fully independent information on emissions for verifying the bottom-up inventories. With the global coverage of satellite observations, DECSO can be easily applied to different regions. After validation of DECSO over regions like Europe, where there is sufficient information of emissions, the added value of DECSO for deriving NH_3 emissions is to provide NH_3 emissions over regions with limited local information of NH_3 emissions.

Data

The CrIS NH_3 data v1.6.4 of SNPP and NOAA-20 created by Environment and Climate Change Canada are currently publicly available upon request (mark.shephard@canada.ca) at

https://hpfx.collab.science.gc.ca/~mas001/satellite_ext/cris/snpp/nh3/v1_6_4.

The TROPOMI NO2 data version 2.4 are available via the Copernicus website

https://dataspace.copernicus.eu/ and via the TEMIS website

https://www.temis.nl/airpollution/no2.php (last access: 02 August 2024)

(https://doi.org/10.5270/S5P-9bnp8q8).

534 The NH$_3$ and NO$_x$ emissions of DECSO v6.3 are available on the GlobEmission website

535 https://www.temis.nl/emissions/data.php.

536 HTAP v3 dataset are available on https://edgar.jrc.ec.europa.eu/dataset_htap_v3

537 The European emissions data sets for countries NEC, LRTAP and large facilities E-PRTR are available

538 on the website https://www.eea.europa.eu/en/analysis of the EEA.

539 The CAMS databases CAMS-REG-ANT v5.1, CAMS-GLOB-ANT, CAMS-TEMPO are available on the

540 ECCAD website https://eccad.sedoo.fr/#/metadata/608, https://eccad.sedoo.fr/#/metadata/479,

541 https://eccad.sedoo.fr/#/metadata/487 and https://eccad.sedoo.fr/#/metadata/506.

542 The NH$_3$ observation data from the LML network are available on the RIVM website

543 https://data.rivm.nl/data/luchtmeetnet/.

544 The NH$_3$ observation data from the MAN network are available at https://man.rivm.nl (in Dutch).

545 The Dutch registered NH$_3$ emissions are available at https://data.emissieregistratie.nl/export (in

546 Dutch).

547

548

549 Author contributions

550 JD developed the inversion algorithm of NH$_3$, performed all emission inversions, conducted the

551 analysis and wrote the manuscript. RA and JD made the improvement of the inversion algorithm of

552 NOx. HE developed the superobservation code. ED provided the code for a linearization of the

553 averaging kernels of CrIS. MS provided the CrIS data. RWK provided the NH$_3$ observation data from the

554 MAN and LML networks. MGV provided the CAMS-TEMPO profiles. LT provided suggestions during the

555 research. All authors contributed to the reviewing and editing of the manuscript.

556
557 Competing interests

558 Competing interests

559 The contact author has declared that none of the authors has any competing interests.

560

561 Acknowledgments

562 This the work was financed by the Sentinel EO-based Emission and Deposition Service (SEEDS, Grant

563 ID 101004318) project that has received funding from the European Union's Horizon 2020 research

and innovation programme. Part of the work was funded by the Nationaal Kennisprogramma Stikstof (NKS) of the Dutch Ministry of Agriculture, Nature and Food Quality.

Financial support

This research has been supported by the European Union's Horizon 2020 research and innovation programme (grant no. 101004318).

References

Adams, C., McLinden, C. A., Shephard, M. W., Dickson, N., Dammers, E., Chen, J., Makar, P., Cady-Pereira, K. E., Tam, N., Kharol, S. K., Lamsal, L. N., and Krotkov, N. A.: Satellite-derived emissions of carbon monoxide, ammonia, and nitrogen dioxide from the 2016 Horse River wildfire in the Fort McMurray area, Atmos. Chem. Phys., 19, 2577-2599, 10.5194/acp-19-2577-2019, 2019.

Backes, A., Aulinger, A., Bieser, J., Matthias, V., and Quante, M.: Ammonia emissions in Europe, part I: Development of a dynamical ammonia emission inventory, Atmospheric Environment, 131, 55-66, https://doi.org/10.1016/j.atmosenv.2016.01.041, 2016a.

Backes, A. M., Aulinger, A., Bieser, J., Matthias, V., and Quante, M.: Ammonia emissions in Europe, part II: How ammonia emission abatement strategies affect secondary aerosols, Atmospheric Environment, 126, 153-161, https://doi.org/10.1016/j.atmosenv.2015.11.039, 2016b.

Beer, R., Shephard, M. W., Kulawik, S. S., Clough, S. A., Eldering, A., Bowman, K. W., Sander, S. P., Fisher, B. M., Payne, V. H., Luo, M., Osterman, G. B., and Worden, J. R.: First satellite observations of lower tropospheric ammonia and methanol, Geophysical Research Letters, 35, https://doi.org/10.1029/2008GL033642, 2008.

Behera, S. N., Sharma, M., Aneja, V. P., and Balasubramanian, R.: Ammonia in the atmosphere: a review on emission sources, atmospheric chemistry and deposition on terrestrial bodies, Environmental Science and Pollution Research, 20, 8092-8131, 10.1007/s11356-013-2051-9, 2013.

Berkhout, A. J. C., Swart, D. P. J., Volten, H., Gast, L. F. L., Haaima, M., Verboom, H., Stefess, G., Hafkenscheid, T., and Hoogerbrugge, R.: Replacing the AMOR with the miniDOAS in the ammonia monitoring network in the Netherlands, Atmos. Meas. Tech., 10, 4099-4120, 10.5194/amt-10-4099-2017, 2017.

604 Beusen, A. H. W., Bouwman, A. F., Heuberger, P. S. C., Van Drecht, G., and Van Der Hoek, K.
605 W.: Bottom-up uncertainty estimates of global ammonia emissions from global agricultural
606 production systems, Atmospheric Environment, 42, 6067-6077,
607 https://doi.org/10.1016/j.atmosenv.2008.03.044, 2008.

608

609 Boersma, K. F., Vinken, G. C. M., and Eskes, H. J.: Representativeness errors in comparing
610 chemistry transport and chemistry climate models with satellite UV–Vis tropospheric
611 column retrievals, Geosci. Model Dev., 9, 875-898, 10.5194/gmd-9-875-2016, 2016.

612

613 Buchhorn, M., Smets, B., Bertels, L., De Roo, B., Lesiv, M., Tsendbazar, N.-E., Herold, M., and
614 Fritz, S.: Copernicus Global Land Service: Land Cover 100m: collection 3: epoch 2019: Globe,
615 10.5281/zenodo.3939050, 2020.

616

617 Cao, H., Henze, D. K., Shephard, M. W., Dammers, E., Cady-Pereira, K., Alvarado, M.,
618 Lonsdale, C., Luo, G., Yu, F., Zhu, L., Danielson, C. G., and Edgerton, E. S.: Inverse modeling of
619 NH3 sources using CrIS remote sensing measurements, Environmental Research Letters, 15,
620 104082, 10.1088/1748-9326/abb5cc, 2020.

621

622 Cao, H., Henze, D. K., Zhu, L., Shephard, M. W., Cady-Pereira, K., Dammers, E., Sitwell, M.,
623 Heath, N., Lonsdale, C., Bash, J. O., Miyazaki, K., Flechard, C., Fauvel, Y., Kruit, R. W.,
624 Feigenspan, S., Brümmer, C., Schrader, F., Twigg, M. M., Leeson, S., Tang, Y. S., Stephens, A. C.
625 M., Braban, C., Vincent, K., Meier, M., Seitler, E., Geels, C., Ellermann, T., Sanocka, A., and
626 Capps, S. L.: 4D-Var Inversion of European NH3 Emissions Using CrIS NH3 Measurements and
627 GEOS-Chem Adjoint With Bi-Directional and Uni-Directional Flux Schemes, Journal of
628 Geophysical Research: Atmospheres, 127, e2021JD035687,
629 https://doi.org/10.1029/2021JD035687, 2022.

630

631 Chen, Y., Shen, H., Kaiser, J., Hu, Y., Capps, S. L., Zhao, S., Hakami, A., Shih, J. S., Pavur, G. K.,
632 Turner, M. D., Henze, D. K., Resler, J., Nenes, A., Napelenok, S. L., Bash, J. O., Fahey, K. M.,
633 Carmichael, G. R., Chai, T., Clarisse, L., Coheur, P. F., Van Damme, M., and Russell, A. G.: High-
634 resolution hybrid inversion of IASI ammonia columns to constrain US ammonia emissions
635 using the CMAQ adjoint model, Atmos. Chem. Phys., 21, 2067-2082, 10.5194/acp-21-2067-
636 2021, 2021.

637

638 Clarisse, L., Clerbaux, C., Dentener, F., Hurtmans, D., and Coheur, P.-F.: Global ammonia
639 distribution derived from infrared satellite observations, Nature Geoscience, 2, 479-483,
640 10.1038/ngeo551, 2009.

641

642 Crippa, M., Guizzardi, D., Muntean, M., Schaaf, E., Dentener, F., van Aardenne, J. A., Monni,
643 S., Doering, U., Olivier, J. G. J., Pagliari, V., and Janssens-Maenhout, G.: Gridded emissions of
644 air pollutants for the period 1970–2012 within EDGAR v4.3.2, Earth Syst. Sci. Data, 10, 1987-
645 2013, 10.5194/essd-10-1987-2018, 2018.

646

647 Crippa, M., Guizzardi, D., Butler, T., Keating, T., Wu, R., Kaminski, J., Kuenen, J., Kurokawa, J.,
648 Chatani, S., Morikawa, T., Pouliot, G., Racine, J., Moran, M. D., Klimont, Z., Manseau, P. M.,
649 Mashayekhi, R., Henderson, B. H., Smith, S. J., Suchyta, H., Muntean, M., Solazzo, E., Banja,
650 M., Schaaf, E., Pagani, F., Woo, J. H., Kim, J., Monforti-Ferrario, F., Pisoni, E., Zhang, J., Niemi,

651 D., Sassi, M., Ansari, T., and Foley, K.: The HTAP_v3 emission mosaic: merging regional and
652 global monthly emissions (2000–2018) to support air quality modelling and policies, Earth
653 Syst. Sci. Data, 15, 2667-2694, 10.5194/essd-15-2667-2023, 2023.

655 Dammers, E., McLinden, C. A., Griffin, D., Shephard, M. W., Van Der Graaf, S., Lutsch, E.,
656 Schaap, M., Gainairu-Matz, Y., Fioletov, V., Van Damme, M., Whitburn, S., Clarisse, L., Cady-
657 Pereira, K., Clerbaux, C., Coheur, P. F., and Erisman, J. W.: NH3 emissions from large point
658 sources derived from CrIS and IASI satellite observations, Atmos. Chem. Phys., 19, 12261-
659 12293, 10.5194/acp-19-12261-2019, 2019.

661 Ding, J., van der A, R. J., Mijling, B., and Levelt, P. F.: Space-based NOx emission estimates
662 over remote regions improved in DECSO, Atmos. Meas. Tech., 10, 925-938, 10.5194/amt-10-
663 925-2017, 2017a.

665 Ding, J., van der A, R. J., Mijling, B., Levelt, P. F., and Hao, N.: NOx emission estimates during
666 the 2014 Youth Olympic Games in Nanjing, Atmos. Chem. Phys., 15, 9399-9412,
667 10.5194/acp-15-9399-2015, 2015.

669 Ding, J., van der A, R., Mijling, B., de Laat, J., Eskes, H., and Boersma, K. F.: NOx emissions in
670 India derived from OMI satellite observations, Atmospheric Environment: X, 14, 100174,
671 https://doi.org/10.1016/j.aeaoa.2022.100174, 2022.

673 Ding, J., van der A, R. J., Eskes, H. J., Mijling, B., Stavrakou, T., van Geffen, J. H. G. M., and
674 Veefkind, J. P.: NOx Emissions Reduction and Rebound in China Due to the COVID-19 Crisis,
675 Geophysical Research Letters, 47, e2020GL089912, 10.1029/2020GL089912, 2020.

677 Ding, J., Miyazaki, K., van der A, R. J., Mijling, B., Kurokawa, J. I., Cho, S., Janssens-Maenhout,
678 G., Zhang, Q., Liu, F., and Levelt, P. F.: Intercomparison of NOx emission inventories over East
679 Asia, Atmos. Chem. Phys., 17, 10125-10141, 10.5194/acp-17-10125-2017, 2017b.

681 EEA: Emissions of the main air pollutants in Europe,
682 https://www.eea.europa.eu/en/analysis/indicators/emissions-of-the-main-
683 air?activeAccordion=ecdb3bcf-bbe9-4978-b5cf-0b136399d9f8, last access: 3 April, 2024.

685 EPRTR: European Pollutant Release and Transfer Register, database version v4.2 [dataset],
686 http://prtr.ec.europa.eu/,2012.

688 Erisman, J. W., Sutton, M. A., Galloway, J., Klimont, Z., and Winiwarter, W.: How a century of
689 ammonia synthesis changed the world, Nature Geoscience, 1, 636-639, 10.1038/ngeo325,
690 2008.

692 Erisman, J. W., Galloway, J. N., Seitzinger, S., Bleeker, A., Dise, N. B., Petrescu, A. M. R., Leach,
693 A. M., and de Vries, W.: Consequences of human modification of the global nitrogen cycle,
694 Philosophical Transactions of the Royal Society B: Biological Sciences, 368, 20130116,
695 doi:10.1098/rstb.2013.0116, 2013.

Eskes, H. J. and Eichmann, K.-U.: S5P Mission Performance Centre Nitrogen Dioxide [L2__NO2___] Readme, Tech.rep., ESA, https://sentinel.esa.int/documents/247904/3541451/Sentinel-5P-Nitrogen-Dioxide-Level-2-Product-Readme-File, 2022.

Galloway, J. N., Townsend, A. R., Erisman, J. W., Bekunda, M., Cai, Z., Freney, J. R., Martinelli, L. A., Seitzinger, S. P., and Sutton, M. A.: Transformation of the Nitrogen Cycle: Recent Trends, Questions, and Potential Solutions, Science, 320, 889-892, doi:10.1126/science.1136674, 2008.

Ge, X., Schaap, M., Kranenburg, R., Segers, A., Reinds, G. J., Kros, H., and de Vries, W.: Modeling atmospheric ammonia using agricultural emissions with improved spatial variability and temporal dynamics, Atmos. Chem. Phys., 20, 16055-16087, 10.5194/acp-20-16055-2020, 2020.

Gu, B., Zhang, L., Van Dingenen, R., Vieno, M., Van Grinsven, H. J., Zhang, X., Zhang, S., Chen, Y., Wang, S., Ren, C., Rao, S., Holland, M., Winiwarter, W., Chen, D., Xu, J., and Sutton, M. A.: Abating ammonia is more cost-effective than nitrogen oxides for mitigating $PM_{2.5}$ air pollution, Science, 374, 758-762, doi:10.1126/science.abf8623, 2021.

Guevara, M., Jorba, O., Tena, C., Denier van der Gon, H., Kuenen, J., Elguindi, N., Darras, S., Granier, C., and Pérez García-Pando, C.: Copernicus Atmosphere Monitoring Service TEMPOral profiles (CAMS-TEMPO): global and European emission temporal profile maps for atmospheric chemistry modelling, Earth Syst. Sci. Data, 13, 367-404, 10.5194/essd-13-367-2021, 2021.

Han, Y., Revercomb, H., Cromp, M., Gu, D., Johnson, D., Mooney, D., Scott, D., Strow, L., Bingham, G., Borg, L., Chen, Y., DeSlover, D., Esplin, M., Hagan, D., Jin, X., Knuteson, R., Motteler, H., Predina, J., Suwinski, L., Taylor, J., Tobin, D., Tremblay, D., Wang, C., Wang, L., Wang, L., and Zavyalov, V.: Suomi NPP CrIS measurements, sensor data record algorithm, calibration and validation activities, and record data quality, Journal of Geophysical Research: Atmospheres, 118, 12,734-712,748, https://doi.org/10.1002/2013JD020344, 2013.

Hoesly, R. M., Smith, S. J., Feng, L., Klimont, Z., Janssens-Maenhout, G., Pitkanen, T., Seibert, J. J., Vu, L., Andres, R. J., Bolt, R. M., Bond, T. C., Dawidowski, L., Kholod, N., Kurokawa, J. I., Li, M., Liu, L., Lu, Z., Moura, M. C. P., O'Rourke, P. R., and Zhang, Q.: Historical (1750–2014) anthropogenic emissions of reactive gases and aerosols from the Community Emissions Data System (CEDS), Geosci. Model Dev., 11, 369-408, 10.5194/gmd-11-369-2018, 2018.

Janssens-Maenhout, G., Crippa, M., Guizzardi, D., Muntean, M., Schaaf, E., Dentener, F., Bergamaschi, P., Pagliari, V., Olivier, J. G. J., Peters, J. A. H. W., van Aardenne, J. A., Monni, S., Doering, U., Petrescu, A. M. R., Solazzo, E., and Oreggioni, G. D.: EDGAR v4.3.2 Global Atlas of the three major greenhouse gas emissions for the period 1970–2012, Earth Syst. Sci. Data, 11, 959-1002, 10.5194/essd-11-959-2019, 2019.

Kuenen, J., Dellaert, S., Visschedijk, A., Jalkanen, J. P., Super, I., and Denier van der Gon, H.: CAMS-REG-v4: a state-of-the-art high-resolution European emission inventory for air quality modelling, Earth Syst. Sci. Data, 14, 491-515, 10.5194/essd-14-491-2022, 2022.

Kuttippurath, J., Patel, V. K., Kashyap, R., Singh, A., and Clerbaux, C.: Anomalous increase in global atmospheric ammonia during COVID-19 lockdown: Need policies to curb agricultural emissions, Journal of Cleaner Production, 434, 140424, https://doi.org/10.1016/j.jclepro.2023.140424, 2024.

Li, C., Martin, R. V., Shephard, M. W., Cady-Pereira, K., Cooper, M. J., Kaiser, J., Lee, C. J., Zhang, L., and Henze, D. K.: Assessing the Iterative Finite Difference Mass Balance and 4D-Var Methods to Derive Ammonia Emissions Over North America Using Synthetic Observations, Journal of Geophysical Research: Atmospheres, 124, 4222-4236, https://doi.org/10.1029/2018JD030183, 2019.

Liu, F., van der A, R. J., Eskes, H., Ding, J., and Mijling, B.: Evaluation of modeling NO_2 concentrations driven by satellite-derived and bottom-up emission inventories using in situ measurements over China, Atmos. Chem. Phys., 18, 4171-4186, 10.5194/acp-18-4171-2018, 2018.

Lolkema, D. E., Noordijk, H., Stolk, A. P., Hoogerbrugge, R., van Zanten, M. C., and van Pul, W. A. J.: The Measuring Ammonia in Nature (MAN) network in the Netherlands, Biogeosciences, 12, 5133-5142, 10.5194/bg-12-5133-2015, 2015.

Luo, Z., Zhang, Y., Chen, W., Van Damme, M., Coheur, P. F., and Clarisse, L.: Estimating global ammonia (NH3) emissions based on IASI observations from 2008 to 2018, Atmos. Chem. Phys., 22, 10375-10388, 10.5194/acp-22-10375-2022, 2022.

Menut, L., Bessagnet, B., Briant, R., Cholakian, A., Couvidat, F., Mailler, S., Pennel, R., Siour, G., Tuccella, P., Turquety, S., and Valari, M.: The CHIMERE v2020r1 online chemistry-transport model, Geosci. Model Dev., 14, 6781-6811, 10.5194/gmd-14-6781-2021, 2021.

Menut, L., Bessagnet, B., Khvorostyanov, D., Beekmann, M., Blond, N., Colette, A., Coll, I., Curci, G., Foret, G., Hodzic, A., Mailler, S., Meleux, F., Monge, J. L., Pison, I., Siour, G., Turquety, S., Valari, M., Vautard, R., and Vivanco, M. G.: CHIMERE 2013: a model for regional atmospheric composition modelling, Geosci. Model Dev., 6, 981-1028, 10.5194/gmd-6-981-2013, 2013.

Mijling, B. and van der A, R. J.: Using daily satellite observations to estimate emissions of short-lived air pollutants on a mesoscopic scale, Journal of Geophysical Research: Atmospheres, 117, 10.1029/2012JD017817, 2012.

Mijling, B., van der A, R. J., and Zhang, Q.: Regional nitrogen oxides emission trends in East Asia observed from space, Atmos. Chem. Phys., 13, 12003-12012, 10.5194/acp-13-12003-2013, 2013.

Noordijk, H., Braam, M., Rutledge-Jonker, S., Hoogerbrugge, R., Stolk, A. P., and van Pul, W. A. J.: Performance of the MAN ammonia monitoring network in the Netherlands, Atmospheric Environment, 228, 117400, https://doi.org/10.1016/j.atmosenv.2020.117400, 2020.

Pinterits, M., B. Ullrich, T. Bartmann and M. Gager: European Union emission inventory report 1990-2019 under the UNECE Convention on Long-range Transboundary Air Pollution (Air Convention), EEA Report No 5/2021, 2021NEC, Air pollution in Europe: 2023 reporting status under the National Emission reduction Commitments Directive, 2023 (https://www.eea.europa.eu/publications/national-emission-reduction-commitments-directive-2023/air-pollution-in-europe-2023), 2023.

Renard, J. J., Calidonna, S. E., and Henley, M. V.: Fate of ammonia in the atmosphere—a review for applicability to hazardous releases, Journal of Hazardous Materials, 108, 29-60, https://doi.org/10.1016/j.jhazmat.2004.01.015, 2004.

Rijsdijk, P., Eskes, H., Dingemans, A., Boersma, F., Sekiya, T., Miyazaki, K., and Houweling, S.: Quantifying uncertainties of satellite NO2 superobservations for data assimilation and model evaluation, EGUsphere, 2024, 1-42, 10.5194/egusphere-2024-632, 2024.

Schaap, M., van Loon, M., ten Brink, H. M., Dentener, F. J., and Builtjes, P. J. H.: Secondary inorganic aerosol simulations for Europe with special attention to nitrate, Atmos. Chem. Phys., 4, 857-874, 10.5194/acp-4-857-2004, 2004.

Shephard, M. W. and Cady-Pereira, K. E.: Cross-track Infrared Sounder (CrIS) satellite observations of tropospheric ammonia, Atmos. Meas. Tech., 8, 1323-1336, 10.5194/amt-8-1323-2015, 2015.

Shephard, M. W., Dammers, E., Cady-Pereira, K. E., Kharol, S. K., Thompson, J., Gainariu-Matz, Y., Zhang, J., McLinden, C. A., Kovachik, A., Moran, M., Bittman, S., Sioris, C. E., Griffin, D., Alvarado, M. J., Lonsdale, C., Savic-Jovcic, V., and Zheng, Q.: Ammonia measurements from space with the Cross-track Infrared Sounder: characteristics and applications, Atmos. Chem. Phys., 20, 2277-2302, 10.5194/acp-20-2277-2020, 2020.

Sitwell, M., Shephard, M. W., Rochon, Y., Cady-Pereira, K., and Dammers, E.: An ensemble-variational inversion system for the estimation of ammonia emissions using CrIS satellite ammonia retrievals, Atmos. Chem. Phys., 22, 6595-6624, 10.5194/acp-22-6595-2022, 2022.

Soulie, A., C. Granier, S. Darras, N. Zilbermann, T. Doumbia, M. Guevara, J.-P. Jalkanen, S. Keita, C. Liousse, M. Crippa, D. Guizzardi, R. Hoesly, and Smith, S. J.: Global Anthropogenic Emissions (CAMS-GLOB-ANT) for the Copernicus Atmosphere Monitoring Service Simulations of Air Quality Forecasts and Reanalyses, Earth Syst. Sci. Data, 2023.

Van Damme, M., Clarisse, L., Whitburn, S., Hadji-Lazaro, J., Hurtmans, D., Clerbaux, C., and Coheur, P.-F.: Industrial and agricultural ammonia point sources exposed, Nature, 564, 99-103, 10.1038/s41586-018-0747-1, 2018.

836 Van Damme, M., Clarisse, L., Franco, B., Sutton, M. A., Erisman, J. W., Wichink Kruit, R., van
837 Zanten, M., Whitburn, S., Hadji-Lazaro, J., Hurtmans, D., Clerbaux, C., and Coheur, P.-F.:
838 Global, regional and national trends of atmospheric ammonia derived from a decadal (2008–
839 2018) satellite record, Environmental Research Letters, 16, 055017, 10.1088/1748-
840 9326/abd5e0, 2021.

842 van der A, R. J., Ding, J., and Eskes, H.: Monitoring European anthropogenic NOx emissions
843 from space, Atmos. Chem. Phys., 24, 7523-7534, 10.5194/acp-24-7523-2024, 2024.

845 van der A, R. J., de Laat, A. T. J., Ding, J., and Eskes, H. J.: Connecting the dots: NOx emissions
846 along a West Siberian natural gas pipeline, npj Climate and Atmospheric Science, 3, 16,
847 10.1038/s41612-020-0119-z, 2020.

849 van der A, R. J., Mijling, B., Ding, J., Koukouli, M. E., Liu, F., Li, Q., Mao, H., and Theys, N.:
850 Cleaning up the air: effectiveness of air quality policy for SO2 and NOx emissions in China,
851 Atmos. Chem. Phys., 17, 1775-1789, 10.5194/acp-17-1775-2017, 2017.

853 van der Graaf, S., Dammers, E., Segers, A., Kranenburg, R., Schaap, M., Shephard, M. W., and
854 Erisman, J. W.: Data assimilation of CrIS NH3 satellite observations for improving
855 spatiotemporal NH3 distributions in LOTOS-EUROS, Atmos. Chem. Phys., 22, 951-972,
856 10.5194/acp-22-951-2022, 2022.

858 van Geffen, J. H. G. M., Eskes, H. J., Boersma, K. F., and Veefkind, J. P.: TROPOMI ATBD of the
859 total and tropospheric NO2 data products, Report S5P-KNMI-L2-0005-RP, version 2.4.0,
860 202207-11, KNMI, De Bilt, The Netherlands,,
861 https://sentinel.esa.int/documents/247904/2476257/Sentinel-5P-TROPOMI-ATBD-NO2-
862 data-products (last access: 23 Nov. 2023), 2022.

864 Veefkind, J. P., Aben, I., McMullan, K., Förster, H., de Vries, J., Otter, G., Claas, J., Eskes, H. J.,
865 de Haan, J. F., Kleipool, Q., van Weele, M., Hasekamp, O., Hoogeveen, R., Landgraf, J., Snel,
866 R., Tol, P., Ingmann, P., Voors, R., Kruizinga, B., Vink, R., Visser, H., and Levelt, P. F.: TROPOMI
867 on the ESA Sentinel-5 Precursor: A GMES mission for global observations of the atmospheric
868 composition for climate, air quality and ozone layer applications, Remote Sensing of
869 Environment, 120, 70-83, http://dx.doi.org/10.1016/j.rse.2011.09.027, 2012.

871 White, E., Shephard, M. W., Cady-Pereira, K. E., Kharol, S. K., Ford, S., Dammers, E., Chow, E.,
872 Thiessen, N., Tobin, D., Quinn, G., O'Brien, J., and Bash, J.: Accounting for Non-Detects:
873 Application to Satellite Ammonia Observations, Remote Sensing, 15, 2610, 2023.

875 Wyer, K. E., Kelleghan, D. B., Blanes-Vidal, V., Schauberger, G., and Curran, T. P.: Ammonia
876 emissions from agriculture and their contribution to fine particulate matter: A review of
877 implications for human health, Journal of Environmental Management, 323, 116285,
878 https://doi.org/10.1016/j.jenvman.2022.116285, 2022.

880 Zavyalov, V., Esplin, M., Scott, D., Esplin, B., Bingham, G., Hoffman, E., Lietzke, C., Predina, J.,
881 Frain, R., Suwinski, L., Han, Y., Major, C., Graham, B., and Phillips, L.: Noise performance of

the CrIS instrument, Journal of Geophysical Research: Atmospheres, 118, 13,108-113,120, https://doi.org/10.1002/2013JD020457, 2013.

Zhang, L., Chen, Y., Zhao, Y., Henze, D. K., Zhu, L., Song, Y., Paulot, F., Liu, X., Pan, Y., Lin, Y., and Huang, B.: Agricultural ammonia emissions in China: reconciling bottom-up and top-down estimates, Atmos. Chem. Phys., 18, 339-355, 10.5194/acp-18-339-2018, 2018.

Zhang, X., Gu, B., van Grinsven, H., Lam, S. K., Liang, X., Bai, M., and Chen, D.: Societal benefits of halving agricultural ammonia emissions in China far exceed the abatement costs, Nature Communications, 11, 4357, 10.1038/s41467-020-18196-z, 2020.

Zhu, L., Henze, D. K., Cady-Pereira, K. E., Shephard, M. W., Luo, M., Pinder, R. W., Bash, J. O., and Jeong, G.-R.: Constraining U.S. ammonia emissions using TES remote sensing observations and the GEOS-Chem adjoint model, Journal of Geophysical Research: Atmospheres, 118, 3355-3368, https://doi.org/10.1002/jgrd.50166, 2013.